A sodium-directed photon-induced assembly strategy for preparing multi-site catalysts with high atomic utilization efficiency

Xiaoqiang An[*,a,#], Tingcha Wei[a,b,#], Peijia Ding[c], Li-Min Liu[*,c], Lunqiao Xiong[d], Junwang Tang[*,d], Jiani Ma[e], Feng Wang[f], Huijuan Liu[a], Jiuhui Qu[a]

[a] Center for Water and Ecology, State Key Joint Laboratory of Environment Simulation and Pollution Control, School of Environment, Tsinghua University, Beijing 100084, China

[b] MIIT Key Laboratory of Aerospace Information Materials and Physics, College of Physics, Nanjing University of Aeronautics and Astronautics, Nanjing 211106, China

[c] School of Physics, Beihang University, Beijing 100191, China

[d] Department of Chemical Engineering, University College London, Torrington Place, London WC1E 7JE, UK

[e] Key Laboratory of Applied Surface and Colloid Chemistry, Ministry of Education, School of Chemistry and Chemical Engineering, Shanxi Normal University, Xi'an 710119, China

[f] Department of Physics, Chemistry and Biology (IFM), Linköping University, Linköping 581 83, Sweden

Abstract: Integrating different reaction sites offers new prospects to address the difficulties in single-atom catalysis, but the atomic-precision regulation of active sites remains challenging. Here, we demonstrate a sodium-directed photon-induced assembly (SPA) strategy for boosting the atomic utilization efficiency of single-atom catalysts (SACs) by constructing multifarious Au sites on TiO_2 substrate. Na^+ was employed as the crucial cement to direct Au single atoms onto TiO_2, while the light-induced electron transfer from excited TiO_2 to Au(Na^+) ensembles contributed to the

self-assembly formation of Au nanoclusters. The synergism between plasmonic near-field and Schottky junction enabled the cascade electron transfer for charge separation, which was further enhanced by oxygen vacancies in TiO_2. Our dual-site photocatalysts exhibited a nearly two orders of magnitude improvement in the hydrogen evolution activity under simulated solar light, with a striking TOF value of 1533 h^{-1} that exceeded other Au/TiO_2-based photocatalysts reported. Our SPA strategy can be easily extended to prepare a wide range of metal-coupled nanostructures with enhanced performance for diverse catalytic reactions. Thus, this study provides a well-defined platform to extend the boundaries of SACs for multi-site catalysis through harnessing metal-support interactions.

KEYWORDS: Bottom-up assembly; single-atom catalysts; atomic utilization efficiency; water splitting; metal-support interactions

Introduction

Single-atom catalysts (SACs) have attracted considerable attention in recent years because of the high utilization efficiency of metal atoms, especially for noble metals that usually act as highly reactive sites for catalytic reactions.[1] Despite the very encouraging progress in the past few years, there are still several challenges to be addressed. Firstly, due to the simplicity of the single-atom center, it is difficult to break the limit of the scaling relations among multistep catalytic reactions.[2] The performance of SACs is far from the theoretical maximum efficiency of atomic utilization. Secondly, single atoms with high surface energy are susceptible to agglomeration, posing a significant challenge to catalyst stability for further development.[3]

Recent exploration suggests that the above issues can be addressed by introducing combined multifunction atomic sites in SACs, such as dual-metal dimers, single-atom alloys, and nanoclusters.[4-5] In these protocols, coupling between different atomic sites can induce the redistribution of metal charges and optimize the adsorption/desorption of multi-intermediates, thereby effectively decreasing the reaction energy barriers for intriguing performance.[6] However, a significant challenge in developing this kind of catalyst is the difficulty of simultaneously anchoring multifarious sites on the same substrate and controlling their interactions under synthesis conditions.[7] Given this, a general strategy that can modulate atomically dispersed metals is urgently required for the construction of multi-site catalysts.

As one of the most important concepts in heterogeneous catalysis, metal-support interactions have received much attention in recent years. It has been revealed that the

unique interfacial interactions have a substantial influence on the coordination structure of dispersed metal atoms and become one of the few tools able to modify the spatial distribution of active sites on a support material.[8] This means that one can on-site refine SACs by assembling the post-deposited metal atoms into the desired derivatives via controlling the metal-support interactions, providing a facile bottom-up way to construct the mentioned multi-site catalysts. Nevertheless, manipulating the dispersion of metal atoms and realizing the synergism between multifarious active sites remains a huge challenge.[9]

Inspired by this hypothesis, we develop a sodium-directed photon-induced assembly (denoted SPA) strategy to construct multifarious atomic sites on 001-faceted TiO_2 nanosheets for synergistic photocatalysis (Figure 1). There are three crucial aspects of this SPA strategy: i) Na^+ is employed as an adherent mediator to regulate the Au-TiO_2 interactions, which could stabilize the proximal Au single atoms on TiO_2 (denoted S-Au/TiO_2) by the strong metal-support interactions (SMSI).[10] ii) The exposure of pre-synthesized powders to light illumination induced the excitation of TiO_2 photocatalysts. The transfer of photo-generated electrons from Ti^{3+} centers to Au(Na^+) ensembles enabled the in-situ assembly of neighboring Au single atoms into nanoclusters with a plasmonic near-field effect.[11] Accordingly, the sample with integrated Au single atoms and nanoclusters is denoted SC-Au/TiO_2. iii) To build up a fast channel for the cascade electron transfer between synergistic sites, vacuum heating of as-synthesized catalysts is performed to create oxygen vacancies (O_v) in TiO_2 supports. As such, the synthesized Au nanoclusters/oxygen-deficient TiO_2/Au single atoms (SC-Au/O_v-TiO_2) catalyst

exhibits a high hydrogen production rate of 4.37 mmol g^{-1} h^{-1} with a TOF value of 1533 h^{-1}, representing the best atom utilization efficiency amongst reported Au/TiO_2 photocatalysts. More importantly, our SPA strategy can be easily extended to prepare a wide range of metal-coupled nanostructures with enhanced performance for diverse catalytic reactions, thus providing a universal methodology for further upgrading SACs.

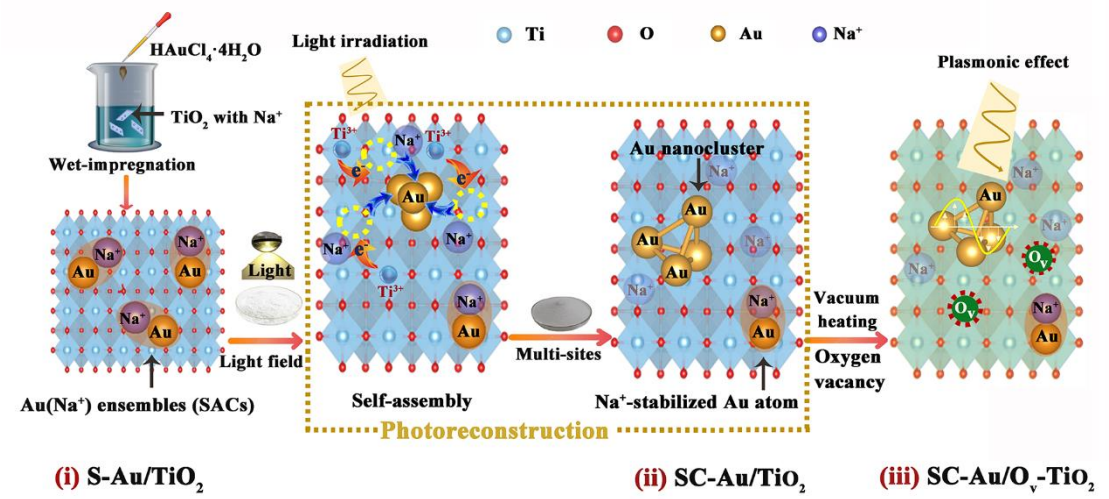

Figure 1. Schematic illustration of the preparation of multi-site catalysts via the photon-induced assembly strategy.

Results and discussion

Photocatalytic properties of site-engineered TiO_2 nanosheets

Photocatalytic hydrogen production was performed to evaluate the activities of atomic-level engineered photocatalysts. Under simulated solar light irradiation, pristine TiO_2 presents poor activity for water splitting, with an H_2 production rate of 0.05 mmol g^{-1} h^{-1} (Figure 2a). The introduction of Au single atoms (0.07 wt% of TiO_2 determined by the inductively coupled plasma optical emission spectrometry (ICP-OES)) as cocatalysts could efficiently improve the activity, leading to a 30-fold increase in the H_2 production rate. Interestingly, the photoreconstructed sample (SC-Au/TiO_2) brings

this to a 60-fold increase compared with TiO_2, revealing the significant contribution of multifarious Au sites to hydrogen production.

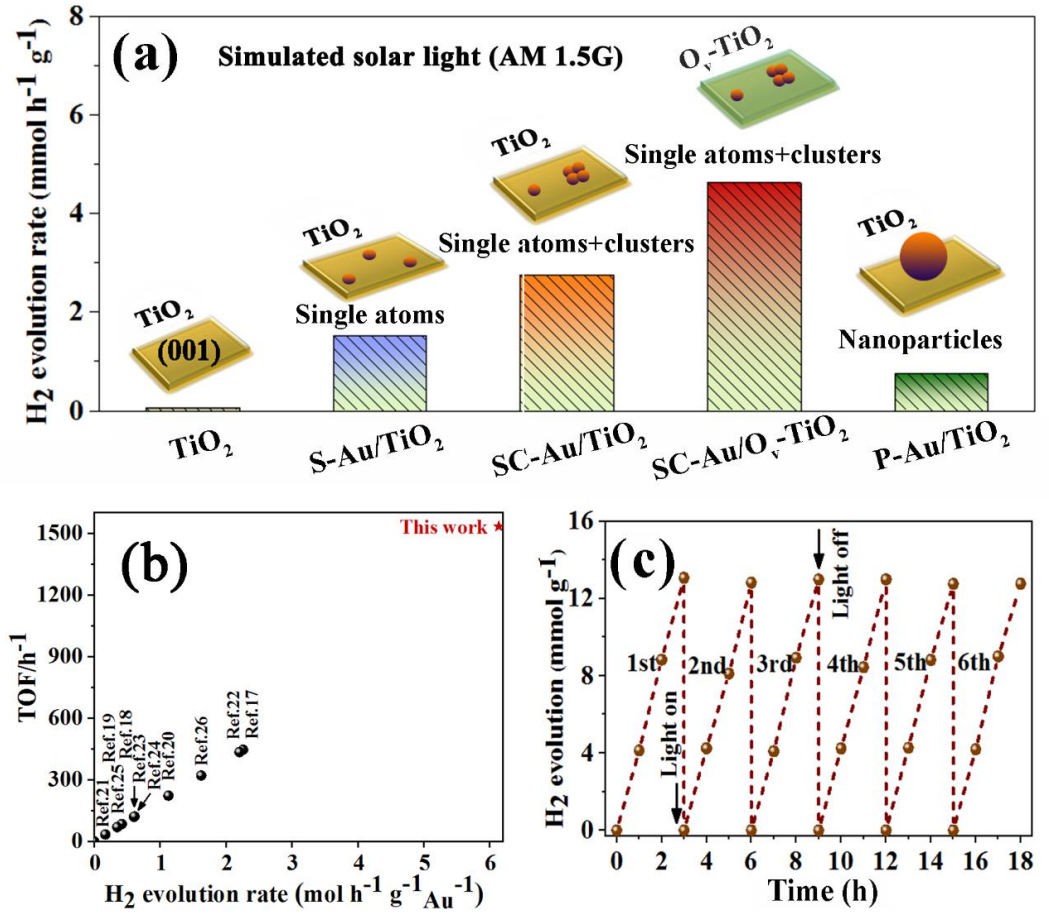

Figure 2. The excellent photocatalytic performance of site-engineered catalysts. (a) Photocatalytic H_2 production over TiO_2 decorated by different types of Au sites under simulated solar light irradiation; (b) Comparing TOF and H_2 evolution rate of SC-Au/O_v-TiO_2 with the presentative Au/TiO_2 photocatalysts; (c) The photocatalytic activity of SC-Au/O_v-TiO_2 for 6 cyclic water splitting runs.

Creating oxygen vacancies (O_v) in TiO_2 supports (confirmed by electron spin resonance spectra, Figure S1) by vacuum heating further doubled the activity, which may be due to the improved charge transfer as discussed below. A striking H_2 generation rate of 4.37 mmol g^{-1} h^{-1} is thus obtained on the final SC-Au/O_v-TiO_2, which is nearly

two orders of magnitude higher than pristine 001-TiO_2 and even 6 times higher than the conventional sample with the same quantity of Au species fabricated via the photodeposition route (P-Au/TiO_2, Figure S2).[12] The turnover frequency (TOF) of SC-Au/O_v-TiO_2 was calculated to evaluate the catalyst activity per Au active site. The value of 1533 h^{-1} is more than two times higher than the benchmark Au/TiO_2 photocatalysts reported (Figure 2b and Table S1).[13-22] Beyond an exceptional atom utilization efficiency, SC-Au/O_v-TiO_2 also exhibits excellent recyclability without any obvious activity degradation (Figure 2c) and structure change after 6 runs (Figure S3). No chemical leaching of Au species into the reaction solution is detected by ICP-OES, revealing the stabilization of atomically dispersed sites.

The overall evolution of atomically dispersed sites

A series of investigations were conducted to explore the mechanism behind the outstanding photoactivity of SC-Au/O_v-TiO_2. X-ray diffraction (XRD, Figure S4) and transmission electron microscopy (TEM, Figure 3a) analyses confirm the formation of anatase TiO_2 nanosheets with exposed {001} facets (Figure S5 and Figure S6). The pretreatment of the resultant sample in NaOH solutions enabled the surface modification of TiO_2 by sodium ions (detailed procedures in Supplementary information). After this pretreatment, the facile wet-impregnation method led to a homogeneous distribution of Au single atoms (individual bright dots) throughout the TiO_2 support in S-Au/TiO_2 as observed by the high-angle annular dark-field scanning transmission electron microscopy (HAADF-STEM) (Figure 3b). Then the site reconstruction resulted in the coexistence of numerous evenly scattered Au atoms and

adjacent ultra-small clusters in SC-Au/TiO_2 (Figure 3c). Based on the theoretical estimation, a cluster with a diameter of 1.4 nm is populated with ca. 90 Au atoms. An insignificant change in atomic dispersion of Au is observed for SC-Au/O_v-TiO_2, indicating the ultra-stability of reconstructed sites during the vacuum heating process (Figure S7).

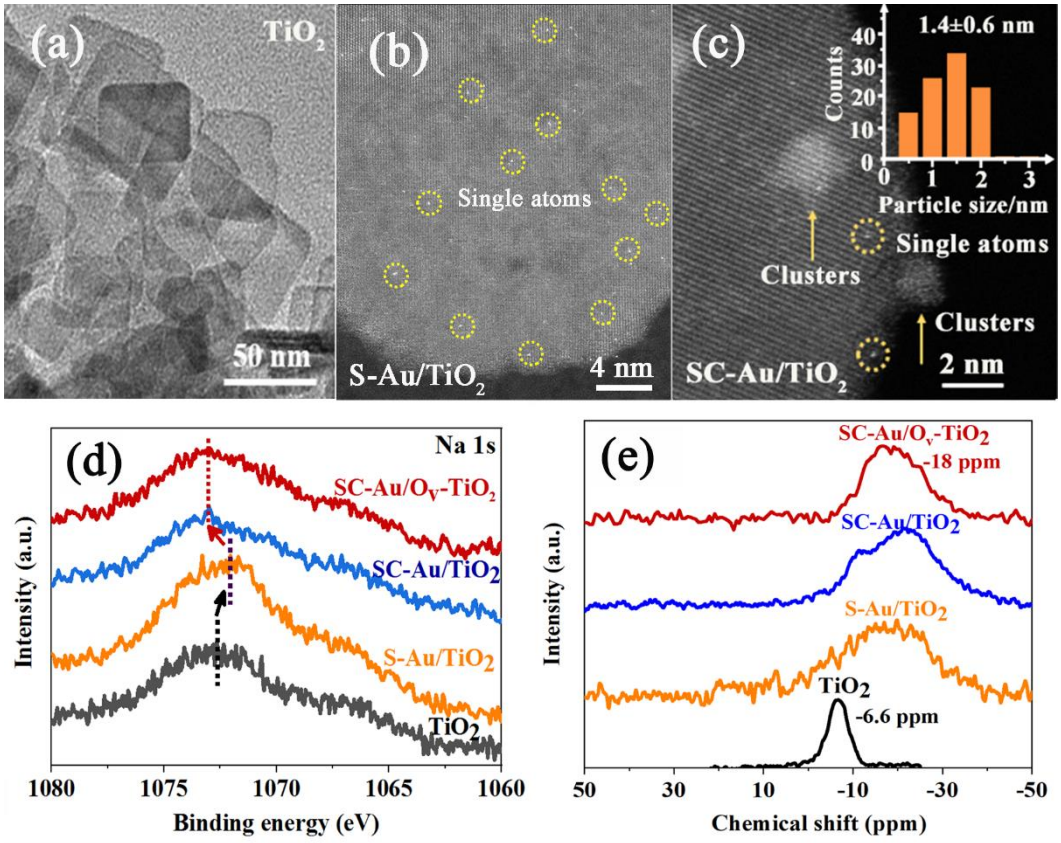

Figure 3. Morphological transformation of atomically dispersed Au sites and the crucial roles of Au/Na^+ interplay. (a) TEM image of TiO_2; (b, c) HAADF-STEM images of S-Au/TiO_2 (b) and SC-Au/TiO_2 (c). Insert of (c) is the size distribution of Au nanoclusters in SC-Au/TiO_2. Single atomic Au sites are highlighted by yellow circles, while cluster sites are highlighted by yellow arrows; (d) XPS spectra of TiO_2, S-Au/TiO_2, SC-Au/TiO_2, and SC-Au/O_v-TiO_2. The introduction of Au single atoms leads to the right shift of Na 1s peak, while photon-induced assembly back-shifts this peak;

(e) ^{23}Na NMR spectra of TiO_2, S-Au/TiO_2, SC-Au/TiO_2, and SC-Au/O_v-TiO_2. The shift of peak toward a higher field indicates the increased electron density of Na^+.

The function of sodium for the immobilization of Au single atoms

The first crucial part of the SPA strategy is the introduction of sodium ions to reconstruct the TiO_2 surface, which acts as a cement to anchor Au single atoms. Although it is technologically challenging to visualize the Na^+ ions, several characterizations confirmed the existence of sodium in all NaOH-impregnated TiO_2 (Figure S8). Combined with the ICP-OES results, the weight content of Na^+ in SC-Au/O_v-TiO_2 is approximately equivalent to that of Au (0.07 wt% of TiO_2). When TiO_2 without NaOH pretreatment was used as a substrate, less amount of Au atoms (0.03 wt% of TiO_2) was anchored (Figure S9). A decreased H_2 evolution rate is observed for the corresponding reconstructed sample (Figure S10), corroborating the crucial roles of Na^+ cement in improving the activity of single atoms.

To clarify the detailed function of Na^+, this interplay was investigated by X-ray photoelectron spectroscopy (XPS), nuclear magnetic resonance (NMR) spectroscopy, and X-ray absorption near-edge structure (XANES). A distinct peak corresponding to the ionic state of Na^+ is observed at the binding energy of 1072 eV in the XPS spectrum of TiO_2 (Figure 3d). This peak shifts to lower bind energy after the introduction of Au single atoms, implying the coupling effect between Au and Na^+.[23] A reversed peak shift toward higher binding energy is observed for SC-Au-TiO_2, thus Na^+ stayed in place during the reconstruction of Au atoms. In the NMR spectra, the shift of the ^{23}Na signal toward a high field suggests the increased electron cloud density of Na^+ caused by Au

loading (Figure 3e). This can also be verified by the normalized Na K-edge XANES spectra (Figure S11). The white line position shifts to lower photon energy after the loading of Au single atoms. Hence, the Au/Na^+ interplay slightly increases the electronic density of Na^+ in Au-loaded samples.[24]

Density functional theory (DFT) calculations were performed to deeply comprehend the role of Na^+ in stabilizing Au single atoms. We found that a single Au atom was prone to be linked to the surface O_{2c} of 001-faceted TiO_2 via an Au-O bond. The modification of TiO_2 by Na^+ decreases the length of the Au-O bond from 3.26 Å to 2.17 Å (Figure S12). It signifies that the shift of the electron cloud from Au to Na^+ could pull Au atoms toward the TiO_2 surface, anchoring these single atoms by forming Au(Na^+) ensembles.[25,26] First-principles molecular dynamics (FPMD) simulation was further carried out to check the stability of the Au(Na^+) ensembles. The initial bond length of Au-Na^+ is determined to be around 2.94 Å. When approaching the (001) facets of TiO_2, the bond length of Au-Na^+ fluctuates periodically in the range of 2.55 Å-3.50 Å (Figure S13), confirming the stabilization of Au(Na^+) ensembles on the support surface.

Reconstruction of Au sites by light illumination

The second crucial part of the SPA strategy is the light-promoted reconstruction of Au single atoms into the combination of nanoclusters and single atoms. We systematically investigated the transformation details by XPS, XANES, and extended X-ray absorption fine structure (EXAFS). In contrast to the metallic state (Au^0) of photo-deposited Au in P-Au/TiO_2, Au single atoms present a positive oxidation state ($Au^{\delta+}$)

in S-Au /TiO_2, as evidenced by the high binding energies of Au $4f_{7/2}$ and Au $4f_{5/2}$ peaks in the XPS spectra (Figure 4a). Light illumination significantly changed the chemical state of Au. The occurrence of metallic state Au (Au^0) in SC-Au/TiO_2 is correlated with the formation of Au nanoclusters through atomic reconstruction, consistent with the observation of Figure 3c. By comparing the peaks area of metallic state Au (Au^0) and oxidation state Au ($Au^{\delta+}$), the contents of Au single atoms and Au nanoclusters in SC-Au/O_v-TiO_2 are estimated to be 63% and 37%, respectively.

The change of coordination environment of Au during the site reconstruction was further confirmed by XANES and EXAFS analyses. For the Fourier transforms (FT) curves of Au L_3-edge in EXAFS in S-Au/TiO_2, the Wavelet transform (WT) maximum corresponding to Au-O bonds is located at 1.6 Å (Figure 4b). Note that this R-space value is ~0.4 Å smaller than the actual one, due to the k dependence of total phase shift.[27] The corrected value of 2.0 Å is very close to the calculated bond length of Au-O in the Na^+-mediated samples (2.17 Å), confirming the stabilization of Au single atoms on the sodium-modified TiO_2.[28] The appearance of Au-O (1.6 Å) and Au-Au (2.5 Å) bonds in SC-Au/TiO_2 and SC-Au/O_v-TiO_2 is consistent with the coexistence of oxidated Au as single atoms and metallic state Au as nanoclusters.

To further look into the underlying mechanism of Au site reconstruction induced by light illumination, in-situ XPS was employed to monitor the chemical environment of Ti in TiO_2 and S-Au-TiO_2 under UV light irradiation. For blank TiO_2, light excitation shifts the Ti 2p peak from 458.7 eV to 458.6 eV (Figure 4c), which could be explained by the generation of delocalized electrons. Interestingly, an inverse peak shift of 0.1 eV

is observed for irradiated S-Au/TiO_2, implying the restructuring of cocatalyst sites via the electron transfer from excited TiO_2 to Au single atoms to form Au nanoclusters.[29,30] This process could also be assessed by the quasi-in-situ electron spin resonance (ESR) experiments. As shown in Figure 4d, pristine TiO_2 exhibits an intense resonance signal at g=2.004 under illumination, attributed to the trapping of photogenerated electrons by oxygen vacancies. However, this signal disappears in S-Au/TiO_2 and a sharp spin peak corresponding to Ti^{3+} emerges at g=1.98 upon illumination.[31] As the illumination time increases, the Ti^{3+} signal weakens and it shifts to g=1.977 when the time is 1 min, confirming the electron transfer from excited TiO_2 to Au single atoms via Ti^{3+}. As such, the continuous irradiation enabled the dynamic reconstruction of Au sites, until reaching an equilibrium between single atoms and nanoclusters, which was significant for the synergistic effect between multifarious atomic sites (Figure S14 and Figure S15).[32]

The impact of dynamic reconstruction on the size of Au clusters and the photoactivity of composite catalysts was investigated. Statistical analysis of HAADF-STEM images reveals that the average diameter of Au clusters increases gradually with the prolonging of irradiation time at the initial stage, while keeping unchanged after 15 minutes of reconstruction (Figure S16). Property evaluation reveals that the 15 minutes sample with an equilibrium state shows the best activity for hydrogen production. Further irradiation treatment deteriorates the photoactivity of SC-Au/TiO_2 (Figure S17), which is presumably caused by the reduction in Ti^{3+} promotive sites for hydrogen evolution reaction (HER) (as discussed below).

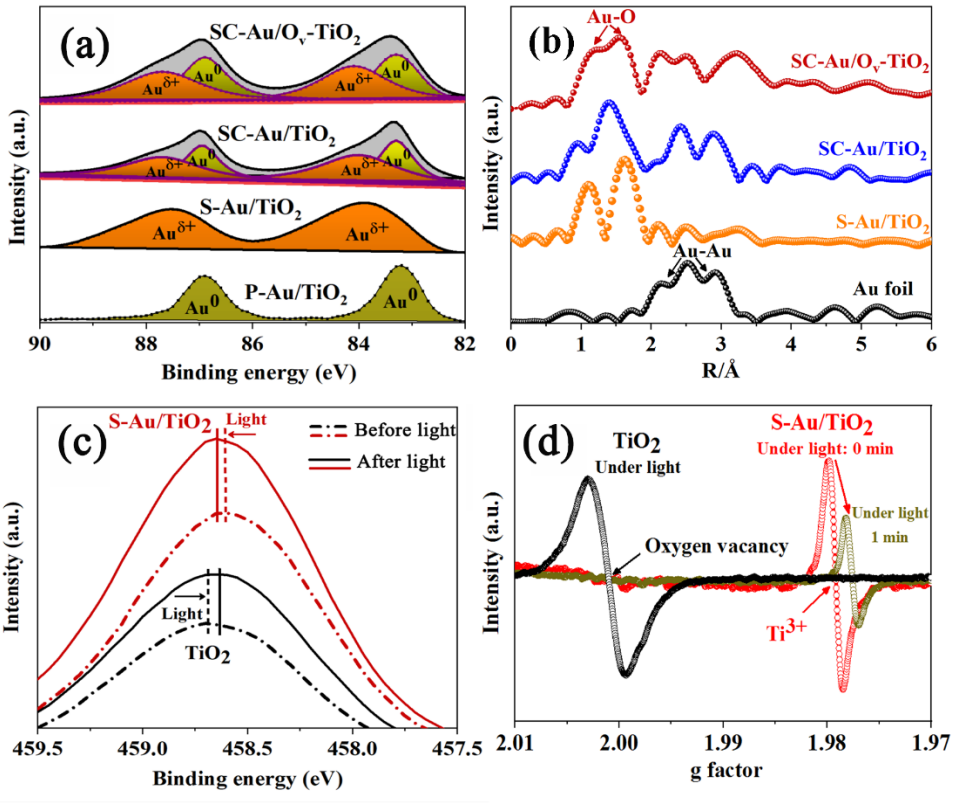

Figure 4. The fundamental mechanism for the reconstruction of atomically dispersed sites. (a) Au 4f XPS spectra of S-Au/TiO_2, SC-Au/TiO_2, SC-Au/O_v-TiO_2 and the reference P-Au/TiO_2; (b) Fourier transform (FT) Au L_3-edge (k) of S-Au/TiO_2, SC-Au/TiO_2, SC-Au/O_v-TiO_2, and the reference Au foil; (c) In-situ Ti 2p XPS spectra of TiO_2 and S-Au/TiO_2 under UV light irradiation; (d) Quasi-in-situ ESR spectra of TiO_2 and S-Au/TiO_2 under UV light irradiation.

The synergy of Au single atoms and nanoclusters for cascade charge transfer

Next, the synergistic effect between multifarious sites in SC-Au/O_v-TiO_2 for charge transfer was investigated. UV-vis reflectance spectra show that the absorption edge of pristine TiO_2 is located around 400 nm, and the introduction of Au single atoms slightly affects the absorption property of TiO_2 (Figure 5a). Reconstruction of Au atoms induces a broad plasmonic absorption peak centered at 550 nm, meanwhile, the color of SC-

Au/TiO_2 turns into dark purple (inset of Figure 5a). This suggests the construction of an oscillating electromagnetic field by bottom-up assembling Au single atoms into nanoclusters, again consistent with the above HAADF-STEM image, in-situ XPS, and ESR spectra of SC-Au/TiO_2. According to the literature, Au clusters (<2 nm) can act as a small bandgap semiconductor, with a Lowest Unoccupied Molecular Orbital (LUMO) level that is more negative than the conduction band (CB) of TiO_2.[33] Thus, the direct transfer of photoexcited electrons from Au nanoclusters to TiO_2 is possible, which was further facilitated by the near-field electromagnetic enhancement.[34] The contribution of the plasmonic field to the performance of reconstructed Au/TiO_2 was further evidenced by the results of visible-light-driven H_2 generation (λ>420 nm). Compared to S-Au/TiO_2 with Au single atoms, the formation of Au nanoclusters in SC-Au/TiO_2 significantly improves the activity by 13 times (Figure S18).

For a better understanding, the three-dimensional finite difference time domain (FDTD) method was used to simulate the near-field distributions of Au nanocluster/TiO_2 junctions (Figure S19). At an excitation wavelength of 350 nm, the electric field of Au nanoclusters is much weaker than that of TiO_2, and the field strength is gradually increased with Au atoms approaching the support surface (Figure 5b). This phenomenon well confirms the feasibility of electron transfer from Au nanoclusters to TiO_2.[35] Consequently, an intensive electric field is centralized at the hetero-interface and spreads over a large area (Figure S20). The UV-induced enhancement of field amplitude is up to 1.8, while visible light (λ=550 nm) further increases the amplitude to 5.5 (Figure S21). Therefore, we conclude that the assembled Au nanoclusters could

not only provide hot electrons for the charge population in TiO_2 but also create an intense near-field to promote interfacial charge separation.[36]

Mott-Schottky analysis was conducted to elucidate the role of Au single atoms in charge separation. The loading of Au single atoms onto TiO_2 positively shifts the flat-band potential (E_{FB}) by 0.13 eV (Figure S22), implying the electron trapping feature of atomically dispersed Au with a low work function by forming a Schottky junction.[37] In contrast, a reverse shift of E_{FB} is observed for SC-Au/TiO_2, which should originate from the elevated Fermi level of Au nanoclusters by forming a plasmonic field.[38] Combining with the aforementioned discussion, we can infer that Au nanoclusters and Au single atoms should possess different affinities for electrons, inducing their different roles as electron donors and reservoirs during charge separation, respectively. [33,39]

Another interesting point was that we found the introduction of oxygen vacancies in TiO_2 support could effectively improve the electron transfer efficiency at the metal/semiconductor interface.[40] The tremendous enhancement can be attributed to the following reasons. Firstly, the positive shift of E_{FB} in the Mott-Schottky plot of SC-Au/O_v-TiO_2 relative to SC-Au/TiO_2 confirms the existence of oxygen defect level in SC-Au/O_v-TiO_2 (Figure S23). It has been well accepted that the oxygen vacancies can decrease the Schottky barrier height (Φ_{SB}) of the Au/TiO_2 junction, which should be favorable for the migration of hot electrons from Au nanoclusters to TiO_2.[41] Secondly, the charge redistribution caused by oxygen vacancies could establish a strong internal electric field at the junction for enhanced charge separation.[42] To validate this deduction, the built-in potential was estimated by the open-circuit potential (V_{oc}) of the

corresponding electrodes under full-spectrum and visible light irradiation. For both cases, SC-Au/O_v-TiO_2 presents the largest V_{oc} under illumination, suggesting efficient charge separation by the internal electric field. For visible light irradiation, the difference between the V_{oc} of SC-Au/TiO_2 and SC-Au/O_v-TiO_2 is much larger than that between S-Au/TiO_2 and SC-Au/TiO_2 (Figure S24), clearly indicating the O_v-enhanced plasmonic effect for activity improvement. This result was also consistent with the enhanced electromagnetic field around Au clusters and defective TiO_2 in the FDTD simulation (Figure S25).[43] Thirdly, it has been well established that defect states caused by oxygen vacancies in TiO_2 can effectively decrease the charge transfer resistance (Figure S26),[44] contributing to the 3-fold increased photoresponse of SC-Au/O_v-TiO_2 than that of pristine SC-Au/TiO_2 (Figure S27).

Taking the above results together, we use a cascade model to elucidate the synergy of Au single atoms and nanoclusters for efficient photocatalysis (Figure 5c). Under light irradiation, the differences in the electron affinities of Au single atoms and Au nanoclusters generate a polarized field to drive the charge separation. Plasmonic Au nanoclusters with a strong near-field effect push the electron density toward TiO_2. The photogenerated electrons from Au nanoclusters and TiO_2 are then collectively transferred to the Na^+-stabilized Au single atoms through the CB of TiO_2. With electron-shuttling capability, oxygen vacancies in TiO_2 could provide an electron "freeway" to facilitate this cascade charge transfer.[45] As such, abundant electrons are populated on Au(Na^+) ensembles to perform the proton reduction reaction, while photoholes left in the valence band of TiO_2 and Au nanoclusters are annihilated by scavengers.[46]

Charge dynamics study of the cascade charge transfer

To better understand the synergistic mechanism, the charge carrier dynamics were investigated by transient absorbance spectra (TAS). As shown in Figure 5d, a positive TAS signal corresponding to photoexcited electrons was probed at wavelength > 470 nm and ps timescale in the spectrum of pristine TiO_2.[47] The introduction of Au single atoms in S-Au/TiO_2 decreases the signal amplitude, suggesting the crucial role of these atomic sites for electron scavenging. However, the redispersion of Au single atoms in SC-Au/TiO_2 and SC-Au/O_v-TiO_2 causes a negative bleach signal below the wavelength of 550 nm, which is indicative of the depletion of plasmon on electrons contributed by the interband transition of self-assembled Au nanoclusters.[48,49] Furthermore, the transient absorption assigned to photoelectrons in the photoreconstructed samples exhibits an obvious increase in the signal amplitude, especially for the SC-Au/O_v-TiO_2 at wavelength >620 nm. This is believed due to the transient accumulation of electrons after the donation of electrons from Au clusters to TiO_2 with the assistance of interfacial electric fields and oxygen vacancies.[50] The decay kinetics of photoelectrons in different samples were further monitored by the time profiles of absorption probed at 650 nm (Figure 5e). Owning to the electron transfer from TiO_2 to Au single atoms, S-Au/TiO_2 displays a shortened lifetime compared to pristine TiO_2. Differently, the lifetime of electrons increases with the occurrence of atomic redispersion, and SC-Au/O_v-TiO_2 has the longest lifetime. These observations can be interpreted as the electron flow from Au clusters to the CB of TiO_2.[51,52]

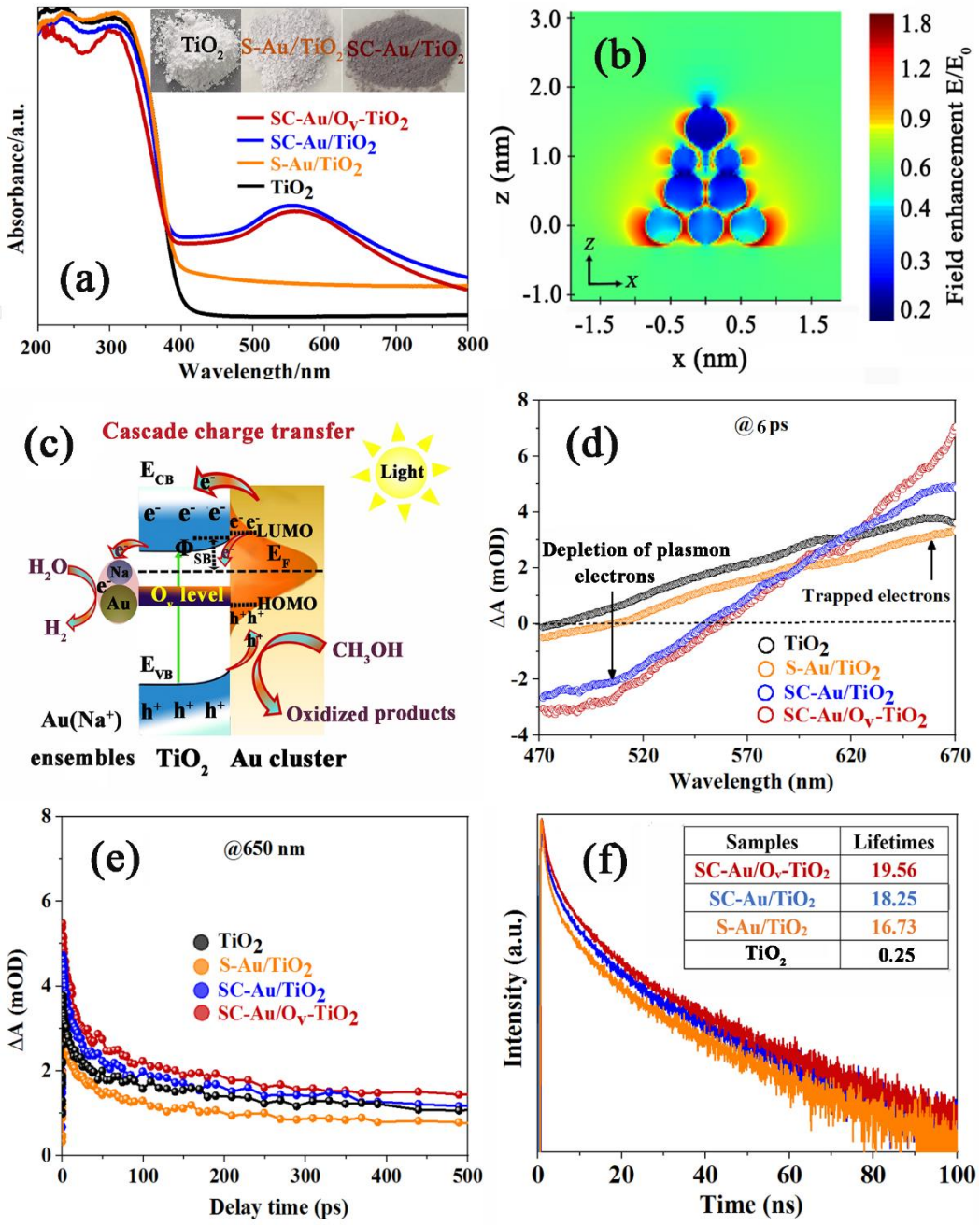

Figure 5. Cascade electron transfer for the efficient charge separation. (a) UV-vis reflectance spectra of TiO_2, S-Au/TiO_2, SC-Au/TiO_2, and SC-Au/O_v-TiO_2. Inserts show the photographs of TiO_2, S-Au/TiO_2, and SC-Au/TiO_2; (b) FDTD simulation of the electric field enhancement over the junction of Au clusters and TiO_2 at an excitation wavelength of 350 nm in the x-z plane. The colored bar shows the electric field intensity normalized by the light source intensity (E/E_0); (c) Schematic illustration of the cascade

charge transfer between Au clusters, TiO_2 and Au single atoms. (d) Transient absorption spectra of TiO_2, S-Au/TiO_2, SC-Au/TiO_2, and SC-Au/O_v-TiO_2 monitored in argon atmosphere after 350 nm excitation; (e) Charge dynamics decay in TiO_2, S-Au/TiO_2, SC-Au/TiO_2, and SC-Au/O_v-TiO_2 monitored at 650 nm; (f) Photoluminescence decay profiles of S-Au/TiO_2, SC-Au/TiO_2, and SC-Au/O_v-TiO_2 in time-correlated single-photon counting (TCSPC).

The suppressed electron/hole recombination was also corroborated by the steady-state and time-resolved photoluminescence (PL) spectroscopic measurements. An intense emission arising from the band-to-band recombination of electron-hole is observed at 425 nm in the spectrum of pristine TiO_2. The noteworthy PL quenching of S-Au/TiO_2 proves the role of singly dispersed Au atoms as the electron reservoir (Figure S28). In good agreement with the activity evaluations, SC-Au/O_v-TiO_2 with synergetic electronic effects exhibits a remarkably prolonged average lifespan of electrons (Figure 5f), validating the effectively suppressed charge recombination (Figure S29).[53]

Theoretic calculations of hydrogen evolution mechanism

Taking the above results together, the synergy driven by the plasmonic near-field and the Schottky junction provided the directional charge-transfer channels, which targeted Au single atoms as active sites for photocatalytic water reduction. As aforementioned, Na^+ cement existed and exhibited a unique interplay with Au single atoms. To understand the contribution of sodium-stabilized Au single atoms for water splitting, the hydrogen adsorption Gibbs free energies (ΔG_H) were examined by theoretical calculations (Figure 6a). As shown in Figure 6b, the adsorption of one H^* onto the

isolated Au forms the structure of Au(H^*) with a ΔG_H value of -1.07 eV. The introduction of one Na^+ dramatically decreases the ΔG_H, with a minimum value of 0.03 eV for Au(Na^+) (H^*). No further improvement is achieved with one more Na^+, confirming the significant contribution of the Au(Na^+) cluster and the ideal ratio of Au to Na^+ for HER activity. To investigate the downhill of ΔG_H, the electronic structure of Au(Na^+)(H^*) was further explored by the density of states (DOS). From the projected density of states (PDOS) for Ti (Figure 6c), a distinct peak corresponding to Ti^{3+} emerges, which could not be observed for a single Au(H^*) on TiO_2 (Figure S30). It indicates the electronic coupling between Au, Na, and Ti, which is in good agreement with the experimental characterizations. According to the PDOS for Au, Na, and H in Au(Na^+) (H^*), the H-s orbital of Au(Na^+)(H^*) is occupied and located at a low energy level relative to the empty orbital of Na^+. With less electronegativity than H, the too-high empty orbit introduced by Na^+ should be the reason for the good HER performance (Figure 6d). Based on these results, we come to the conclusion that sodium not only played a critical role in the stabilization of isolated Au atoms for the construction of multifarious sites but also contributed to the low energy barrier for the water-splitting reaction. Significant catalysis was therefore anticipated for TiO_2-based photocatalysts with more precisely cemented Au(Na^+) ensembles .[44,55]

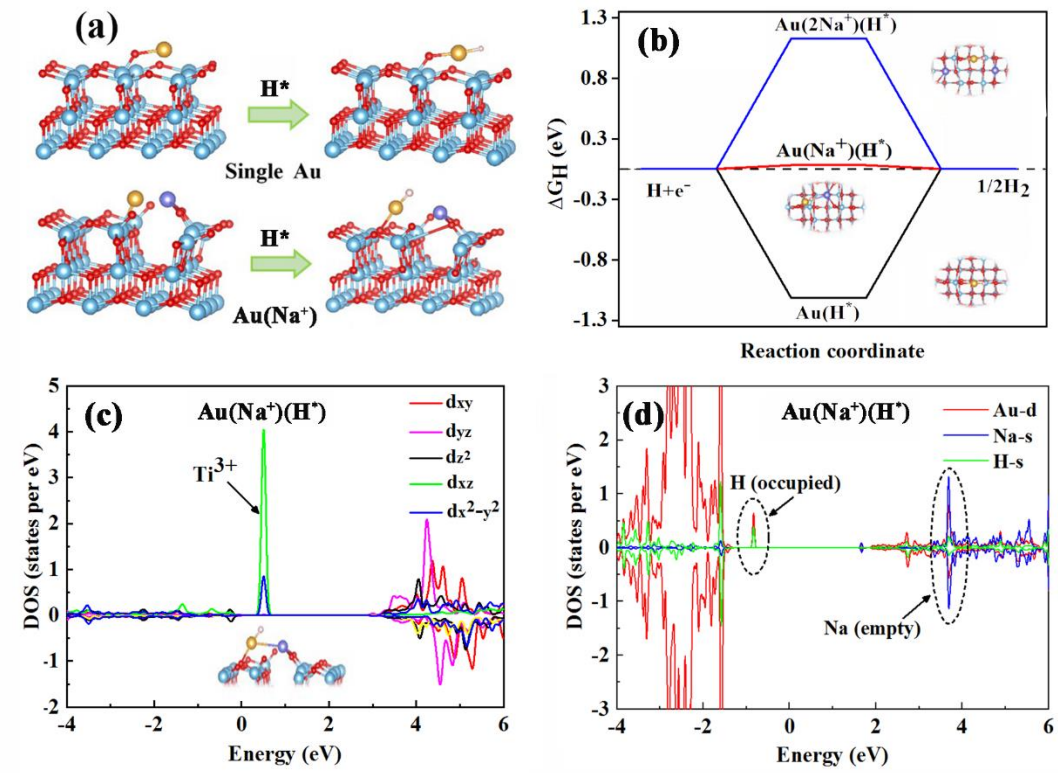

Figure 6. Theoretic verification of Na^+-promoted hydrogen evolution. (a) Local atomic structures of hydrogen adsorption configurations on single Au and Au(Na^+) ensembles. Blue, red, yellow, purple, and white spheres represent Ti, O, Au, Na, and H atoms, respectively. (b) The introduction of one Na^+ could significantly decrease the ΔG_H for HER activity. (c) The Projected DOS of Ti around Au-O bond in Au(Na^+)(H^*). (d) The Projected DOS of Au, Na, and H in Au(Na^+)(H^*).

Extended applications of photon-induced assembly strategy

Inspired by the exciting results of the SPA strategy, we attempted to extend it to a wide range of multi-site synergistic catalysts by either changing the metal oxide supports or noble metals. When combined with other material strategies, such as dual-metal single atoms and facet engineering of support materials (Figure S31), the synergy between single atoms and assembled clusters always contributes to the over-doubled photoactivity of the photoreconstructed catalysts compared to their single atom

counterparts (Figure S32), indicating the vast potential of our SPA strategy for further performance improvement. We further cemented Au single atoms onto BiOBr nanosheets and assembled the neighboring atoms into nanoclusters via the SPA strategy. Compared to S-Au/BiOBr SACs, SC-Au/BiOBr with multifarious sites also exhibits 2 times higher activity for photoconverting N_2 into NH_3 (Figure S33).

The contribution of synergistic sites to thermocatalysis was evaluated by the CO oxidation reaction. Similar to the reported results, the introduction of 0.5 wt% Au single atoms into S-Au/CeO_2 shifts the total CO conversion temperature from 350 to 80 °C.[56] Especially, the complete oxidation of CO at room temperature is easily realized by constructing multifarious Au sites in SC-Au/CeO_2 with the assistance of light-induced assembly (Figure S34). These results well demonstrated the universality of our SPA strategy for the rational design of high-performance SACs.

Conclusions

In summary, by employing a facile sodium-directed photon-induced assembly strategy, the interfacial redispersion of Au single atoms on Na^+-modified defective TiO_2 supports has been designed and rationalized, enabling the formation of multifarious active sites comprising sodium-stabilized Au single atoms and bottom-up assembled Au nanoclusters for efficient photocatalysis. This achieves a prominent advantage of constructing a directional channel for cascade charge transfer from Au nanoclusters to TiO_2 and Au single atoms. Profited from the synergism between the plasmonic near-field and Schottky junction, our multi-site photocatalysts could efficiently reduce water into H_2, with a high TOF value of 1533 h^{-1}. The contributions of sodium cement, light-

induced reassembly, and oxygen vacancies in TiO_2 to the charge separation and water splitting were fundamentally investigated by experimental characterizations and computational simulations. This work not only provides new insights into comprehending and harnessing the metal-support interactions in SACs for activity enhancement but also opens open up new research avenues to construct advanced catalysts with multifarious sites for overcoming the current issues facing SACs.

ASSOCIATED CONTENT

Supporting information. This material is available free of charge via the Internet at http://pubs.acs.org.
Experimental details, additional experimental data and figures, and supplementary discussion.

AUTHOR INFORMATION

Corresponding Authors

* X. An: xqan@tsinghua.edu.cn

* Li-Min Liu: liminliu@buaa.edu.cn

* J. Tang: junwang.tang@ucl.ac.uk

Author Contributions

# X.Q. An and T.C. Wei contributed equally to the experimental work.

Notes

The authors declare no competing financial interest.

Acknowledgment

This work was supported by the National Natural Science Foundation of China (Grant no. 51978372, 52170042, 11974037). We would like to acknowledge the Beijing Synchrotron Radiation Facility (BSRF) for crystal diffraction data collection. This research was supported by the high performance computing (HPC) resources at Beihang University. J. T. and L. X. are also thankful for UK EPSRC (EP/S018204/2), Leverhulme Trust (RPG-2017-122), Royal Society Newton Advanced Fellowship grant (NAF\R1\191163) and Royal Society Leverhulme Trust Senior Research Fellowship (SRF\R1\21000153). The authors thank Y. P. Bi and Y. J. Zhang for the synchronous illumination XPS analysis in Lanzhou Institute of Chemical Physics, Chinese Academy

of Sciences.

References

1. Qiao, B.; Wang, A.; Yang, X.; Allard, L.; Jiang, Z.; Cui, Y.; Liu, J.; Li, J.; Zhang, T. Single-atom catalysis of CO oxidation using Pt_1/FeO_x. *Nature Chem*. **2014**, *3*, 634-641.
2. Pérez-Ramírez, J.; López, N. Strategies to break linear scaling relationships. *Nature Catal.* **2019**, *2*, 971-976.
3. Liu, J.; Tang, Y.; Wang, Y.; Zhang, T.; Li, J. Theoretical understanding of the stability of single-atom catalysts. *Natl. Sci. Rev.* **2018**, *5*, 638-641.
4. Li, X.; Liu, L.; Ren, X.; Gao, J.; Huang, Y.; Liu, B. Microenvironment modulation of single-atom catalysts and their roles in electrochemical energy conversion. *Sci. Adv.* **2020**, *6*, eabb6833.
5. Zhang, L.; Si, R.; Liu, H.; Chen, N.; Wang, Q.; Adair, K.; Wang, Z.; Chen, J.; Song, Z.; Li, J.; Banis, M.; Li, R.; Sham, T.; Gu, M.; Liu, L.; Botton, G.; Sun, X. Atomic layer deposited Pt-Ru dual-metal dimers and identifying their active sites for hydrogen evolution reaction. *Nature Commun.* **2019**, *10*, 4936.
6. Rong, H.; Ji, S.; Zhang, J.; Wang, D.; Li, Y. Synthetic strategies of supported atomic clusters for heterogeneous catalysis. *Nature Commun*. **2020**, *11*, 5884.
7. Xi, W.; Wang, K.; Shen, Y.; Ge, M.; Deng, Z.; Zhao, Y.; Cao, Q.; Ding, Y.; Hu, G.; Luo, J. Dynamic co-catalysis of Au single atoms and nanoporous Au for methane pyrolysism. *Nature Commun.* **2020**, *11*, 1919.
8. Shan, J.; Ye, C.; Jiang, Y.; Jaroniec, M.; Zheng, Y.; Qiao, S. Metal-metal interactions in correlated single-atom catalysts. *Sci. Adv.* **2022**, *8*, eabo0762.

9. Han, B.; Guo, Y.; Huang, Y.e; Xi, W.; Xu, J.; Luo, J.; Qi, H.; Ren, Y.; Liu, X.; Qiao, B.; Zhang, T. Strong metal-support interactions between Pt single atoms and TiO_2. *Angew. Chem. Int. Ed*. **2020**, *59*, 11824-11829.
10. Zhai, Y.; Pierre, D.; Si, R.; Deng, W.; Ferrin, P.; Nilekar, A.; Peng, G.; Herron, J.; Bell, D.; Saltsburg, H.; Mavrikakis, M.; Flytzani-Stephanopoulos, M. Alkali-stabilized Pt-OH_x species catalyze low-temperature water-gas shift reactions. *Science* **2010**, *329*, 1633-1636.
11. Zhang, J.; Wang, H.; Wang, L.; Ali, S.; Wang, C.; Wang, L.; Meng, X.; Li, B.; Su, D.; Xiao, F. Wet-chemistry strong metal-support interactions in titania-supported Au catalysts. *J. Am. Chem. Soc*. **2019**, *141*, 2975-2983.
12. Khan, R.; Naveen, MH.; Abbas, M.; Lee, J.; Kim, H.; Bang, J. Photoelectrochemistry of Au nanocluster-sensitized TiO_2: Intricacy arising from the light-induced transformation of nanoclusters into nanoparticles. *ACS Energy Lett.* **2021**, *6*, 24-32.
13. Naldoni, A.; D'Arienzo, M. Altomare, M.; Marelli, M.; Scotti, R.; Morazzoni, F.; Selli, E.; Dal Santo, V. Pt and Au/TiO_2 photocatalysts for methanol reforming: Role of metal nanoparticles in tuning charge trapping properties and photoefficiency. *Appl. Catal. B-Environ.* **2013**, *130-131*, 239-248.
14. Chang, Y.; Xuan, Y.; Quan, H.; Zhang, H.; Liu, S.; Li, Z.; Yu, K.; Cao, J. Hydrogen treated Au/3DOM-TiO_2 with promoted photocatalytic efficiency for hydrogen evolution from water splitting. *Chem. Eng. J.* **2020**, *382*, 122869.

15. Torras, M.; Molet, P.; Soler, L.; Llorca, J.; Roig, A.; Mihi, A. Au/TiO_2 2D-photonic crystals as UV-visible photocatalysts for H_2 production. *Adv. Energy Mater.* **2022**, *12*, 2103733.

16. Sun, L.; He, X.; Yuan, Y.; Chen, J.; Zhan, W.; Wang, X.; Zhao, Y.; Han, X. Tuning interfacial sequence between nitrogen-doped carbon layer and Au nanoparticles on metal-organic framework-derived TiO_2 to enhance photocatalytic hydrogen production. *Chem. Eng. J.* **2020**, *397*, 125468.

17. Yang, G.; Ding, H.; Chen, D.; Feng, J.; Hao, Q.; Zhu, Y. Construction of urchin-like $ZnIn_2S_4$-Au-TiO_2 heterostructure with enhanced activity for photocatalytic hydrogen evolution. *Appl. Catal. B-Environ.* **2018**, *234*, 260-267.

18. Martínez, L.; Soler, L.; Angurell, I.; Llorca, J. Effect of TiO_2 nanoshape on the photoproduction of hydrogen from water ethanol mixtures over Au_3Cu/TiO_2 prepared with preformed Au-Cu alloy nanoparticles. *Appl. Catal. B-Environ.* **2019**, *248*, 504-514.

19. Ng, S.; Gao, M. Lu, W.; Hong, M.; Ho, G. Selective wavelength enhanced photochemical and photothermal H_2 generation of classical oxide supported metal catalyst. *Adv. Funct. Mater.* **2021**, *31*, 2104750.

20. Jimenez-Calvo, P.; Caps, V.; Ghazzal, M.; Colbeau-Justin, C.; Keller, V. Au/TiO_2 (P25)-gC_3N_4 composites with low gC_3N_4 content enhance TiO_2 sensitization for remarkable H_2 production from water under visible-light irradiation. *Nano Energy* **2020**, *75*, 104888.

21. Marchal, C.; Cottineau, T.; Méndez-Medrano, M.; Colbeau-Justin, C.; Caps, V.; Keller, V. Au/TiO_2-gC_3N_4 nanocomposites for enhanced photocatalytic H_2 production from water under visible light irradiation with very low quantities of sacrificial agents. *Adv. Energy Mater.* **2018**, *8*, 1702142.

22. Al-Azri, Z.; AlOufi, M.; Chan, A.; Waterhouse, G.; Idriss, H. Metal particle size effects on the photocatalytic hydrogen ion reduction. *ACS Catal.* **2019**, *9*, 3946-3958.

23. Suetake, J.; Nosaka, A.; Hodouchi, K.; Matsubara, H.; Nosaka, Y. Characteristics of titanate nanotube and the states of the confined sodium ions. *J. Phys. Chem. C* **2008**, *112*, 18474-18482.

24. Li, J.; Liu, J.; Sun, Q.; Banis, M.; Sun, X.; Sham, T. Tracking the effect of sodium insertion/extraction in amorphous and anatase TiO_2 nanotubes. *J. Phys. Chem. C* **2017**, *121*, 11773-11782.

25. Görlin, M.; Stenlid, J.; Koroidov, S.; Wang, H.; Börner, M.; Shipilin, M.; Kalinko, A.; Murzin, V.; Safonova, O.; Nachtegaal, M.; Uheida, A.; Dutta, J.; Bauer, M.; Nilsson, A.; Diaz-Morales, O. Key activity descriptors of nickel-iron oxygen evolution electrocatalysts in the presence of alkali metal cations. *Nature Commun*. **2020**, *11*, 6181.

26. Yang, M.; Li, S.; Wang, Y.; Herron, J.; Xu, Y.; Allard, L.; Lee, S.; Huang, J.; Mavrikakis, M.; Flytzani-Stephanopoulos, M. Catalytically active Au-$O(OH)_x$ species stabilized by alkali ions on zeolites and mesoporous oxides. *Science* **2014**, *346*, 1498-1501.

27. Wan, J.; Chen, W.; Jia, C.; Zheng, L.; Dong, J.; Zheng, X.; Wang, Y.; Yan, W.; Chen, C.; Peng, Q.; Wang, D.; Li, Y. Defect effects on TiO_2 nanosheets: stabilizing single atomic site Au and promoting catalytic properties. *Adv. Mater*. **2018**, *30*, 1705369.
28. Michalowicz, A.; Girerd, J.; Goulon, J. EXAFS [extended x-ray absorption fine structure] determination of the copper oxalate structure. Relation between structure and magnetic properties. *Inorg. Chem.* **1979**, *18*, 3004-3010.
29. Jiang Z.; Zhang W.; Jin L.; Yang X.; Xu F.; Zhu J.; Huang W. Direct XPS evidence for charge transfer from a reduced rutile TiO_2(110) surface to Au clusters. *J. Phys. Chem. C* **2007**, *111*, 33, 12434–12439.
30. Rodriguez S.; Campbell R.; Goodman D. Electron donor-electron acceptor interactions in bimetallic surfaces: theory and XPS. *J. Phys. Chem.* **1991**, *95*, 5716-5719.
31. Tang, H.; Su, Y.; Zhang, B.; Lee, A. F.; Isaacs, M. A.; Wilson, K.; Li, L.; Ren, Y.; Huang, J.; Haruta, M.; Qiao, B.; Liu, X.; Jin, C.; Su, D.; Wang, J.; Zhang, T. Classical strong metal-support interactions between gold nanoparticles and titanium dioxide. *Sci. Adv.* **2017**, *3*, 1700231.
32. Zhang, Y.; Liu, J.; Qian, K.; Jia, A.; Li, D.; Shi, L.; Hu, J.; Zhu, J.; Huang, W. Structure sensitivity of Au-TiO_2 strong metal-support interactions. *Angew. Chem. Int. Ed.* **2021**, *60*, 12074-12081.
33. Xiao, F.; Zeng, Z.; Liu, B. Bridging the gap: Electron relay and plasmonic sensitization of metal nanocrystals for metal clusters. *J. Am. Chem. Soc*. **2015**, *137*, 10735-10744.

34. Li, L.; Yan, J.; Wang, T.; Zhao, Z.; Zhang, J.; Gong, J.; Guan, N. Sub-10 nm rutile titanium dioxide nanoparticles for efficient visible-light-driven photocatalytic hydrogen production. *Nature Commun*. **2015**, *6*, 5881.

35. Li, C.; Wang, T.; Zhao, Z.; Yang, W.; Li, J.; Li, A.; Yang, Z.; Ozin, G.; Gong, J. Promoted fixation of molecular nitrogen with surface oxygen vacancies on plasmon-enhanced TiO_2 photoelectrodes. *Angew. Chem. Int. Ed*. **2018**, *57*, 5278-5282.

36. Linic, S.; Christophher, P.; Ingram, D. Plasmonic-metal nanostructures for efficient conversion of solar to chemical energy. *Nature Matter*. **2011**, *10*, 911-921.

37. Zhang, Z.; Jiang, X.; Liu, B.; Guo, L.; Lu, N.; Wang, L.; Huang, J.; Liu, K.; Dong, B. IR-driven ultrafast transfer of plasmonic hot electrons in nonmetallic branched heterostructures for enhanced H_2 generation. *Adv. Mater.* **2018**, *30*, 1705221.

38. Khan, R.; Naveen, M.; Abbas, M.; Lee, J.; Kim, H.; Bang, J. Photoelectrochemistry of Au nanocluster-sensitized TiO_2: Intricacy arising from the light-induced transformation of nanoclusters into nanoparticles. *ACS Energy Lett.* **2021**, *6*, 24-32.

39. Zheng, X.; Yan, X.; Ma, J.; Yao, X.; Zhang, J.; Wang, L. Unidirectional/bidirectional electron transfer at the Au/TiO_2 interface operando tracked by SERS spectra from Au and TiO_2. *ACS Appl. Mater. Interfaces* **2021**, *13*, 16498-16506.

40. Chen, X.; Liu, L.; Yu, P.; Mao, S. Increasing solar absorption for photocatalysis with black hydrogenated titanium dioxide nanocrystals. *Science* **2011**, *331*, 746-750.

41. Lin, L.; Feng, X.; Lan, D.; Chen, Y.; Zhong, Q.; Liu, C.; Cheng, Y.; Qi, R.; Ge, J.; Yu, C.; Duan, C.; Huang, R. Coupling effect of Au nanoparticles with the oxygen vacancies of TiO_{2-x} for enhanced charge transfer. *J. Phys. Chem. C* **2020**, *124*, 23823-23831.

42. Zhou Y.; Zhang Z.; Fang Z.; Qiu M.; Ling L.; Long J.; Chen L.; Tong Y.; Su W.; Zhang Y.; Wu J.; Basset J.; Wang X.; Yu G. Defect engineering of metal–oxide interface for proximity of photooxidation and photoreduction. *Proc. Natl. Acad. Sci. USA* **2019**, *116*, 10232-10237.

43. Hüttenhofer, L.; Eckmann, F.; Lauri, A.; Cambiasso, J.; Pensa, E.; Li, Y.; Cortés, E., Sharp, I.; Maier, S. Anapole excitations in oxygen-vacancy-rich TiO_{2-x} nanoresonators: tuning the absorption for photocatalysis in the visible spectrum. *ACS Nano* **2020**, *14*, 2456-2462.

44. Zheng, J.; Lyu, Y.; Wang, R.; Xie, C.; Zhou, H.; Jiang, S.; Wang, S. Crystalline TiO_2 protective layer with graded oxygen defects for efficient and stable silicon-based photocathode. *Nature Commun*. **2018**, *9*, 3572.

45. Wei Z.; Wang H.; Zhang C.; Xu K.; Lu X.; Lu T. Reversed charge transfer and enhanced hydrogen spillover in platinum nanoclusters anchored on titanium oxide with rich oxygen vacancies boost hydrogen evolution reaction. *Angew. Chem. Int. Ed.* **2021**, *133*, 16758-16763.

46. Long, J.; Chang, H.; Gu, Q.; Xu, J.; Fan, L.; Wang, S.; Zhou, Y.; Wei, W.; Huang, L.; Wang, X.; Liu, P.; Huang, W. Gold-plasmon enhanced solar-to-hydrogen

conversion on the {001} facets of anatase TiO_2 nanosheets. *Energy Environ. Sci.* **2014**, *7*, 973-977.

47. Zhang, Y.; Zhao, J.; Wang, H.; Xiao, B.; Zhang, W.; Zhao, X.; Lv, T.; Thangamuthu, M.; Zhang, J.; Guo, Y.; Ma, J.; Lin, L.; Tang, J.; Huang, R.; Liu, Q. Single-atom Cu anchored catalysts for photocatalytic renewable H_2 production with a quantum efficiency of 56%. *Nature Commun.* **2022**, *13*, 58.
48. Li, C.; Li, H.; Wang, S.; Wang, M.; Gao, Y.; Tang, J.; Zhao, S.; Chi, H.; Zhang, P.; Qu, J.; Fan, F. Enhancement in plasmon-induced photoelectrocatalytic water oxidation over Au/TiO_2 with lithium intercalation. *Angew. Chem. Int. Ed*. **2022**, *61*, e202204272.
49. Yi, C.; Tofanelli, M.; Ackerson, C.; Jr, K. Optical properties and electronic energy relaxation of metallic $Au_{144}(SR)_{60}$ nanoclusters. *J. Am. Chem. Soc*. **2013**, *135*, 18222-18228.
50. Zhu, M.; Cai, X.; Fujitsuka, M.; Zhang, J.; Majima, T. $Au/La_2Ti_2O_7$ nanostructures sensitized with black phosphorus for plasmon-enhanced photocatalytic hydrogen production in visible and near-infrared light. *Angew. Chem. Int. Ed.* **2017**, *56*, 2064-2068.
51. Si, Y.; Cao, S.; Wu, Z.; Ji, Y.; Mi, Y.; Wu, X.; Liu, X.; Piao, L. What is the predominant electron transfer process for Au NRs/TiO_2 nanodumbbell heterostructure under sunlight irradiation? *Appl. Catal. B-Environ.* **2018**, *220*, 471-476.

52. Kim, J.; Shi, X.; Jeong, M.; Park, J.; Han, H.; Kim, S.; Guo, Y.; Heinz, T.; Fan, S.; Lee, C.; Park, J.; Zheng, X. Enhancing Mo:$BiVO_4$ solar water splitting with patterned Au nanospheres by plasmon-induced energy transfer. *Adv. Energy Mater.* **2017**, *8*, 1701765.

53. Yu, Y.; Dong, X.; Chen, P.; Geng, Q.; Wang, H.; Li, J.; Zhou, Y.; Dong, F. Synergistic effect of Cu single atoms and Au-Cu alloy nanoparticles on TiO_2 for efficient CO_2 photoreduction. *ACS Nano* **2021**, *15*, 14453-14464.

54. Jin Z.; Li P.; Meng Y.; Fang Z.; Xiao D.; Yu G. Understanding the inter-site distance effect in single-atom catalysts for oxygen electroreduction. *Nature Catal.* **2021**, *4*, 615–622.

55. Xia C.; Qiu Y.; Xia Y.; Zhu P.; King G.; Zhang X.; Wu Z.; Kim J.; Cullen D.; Zheng D.; Li P.; Shakouri M.; Heredia E.; Cui P.; Alshareef H.; Hu Y.; Wang H. General synthesis of single-atom catalysts with high metal loading using graphene quantum dots. *Nature Chem.* **2021**, *13*, 887–894.

56. Zhao, S.; Chen, F.; Duan, S.; Shao, B.; Li, T.; Tang, H.; Lin, Q.; Zhang, J.; Li, L.; Huang, J.; Bion, N.; Liu, W.; Sun, H.; Wang, A.; Haruta, M.; Qiao, B.; Li, J.; Liu, J.; Zhang, T. Remarkable active-site dependent H_2O promoting effect in CO oxidation. *Nature Commun.* **2019**, *10*, 3824.

TOC Graphic

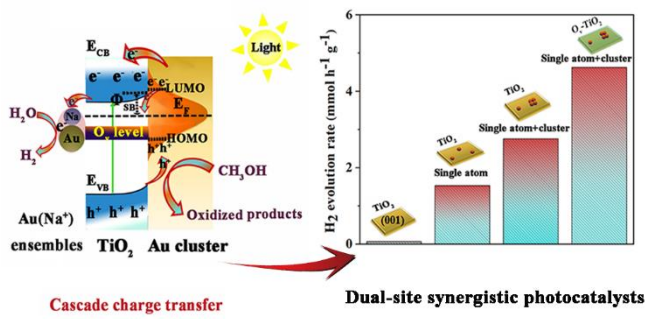

Dual-site synergistic photocatalysts